Electrostatic Double Layer Force between a Sphere and a Planar Substrate in the Presence of Previously Deposited Spherical Particles

Prodip K. Das and Subir Bhattacharjee*

Department of Mechanical Engineering, 4-9 Mechanical Engineering Building, University of Alberta, Edmonton, Alberta T6G 2G8, Canada

Received November 20, 2004. In Final Form: February 26, 2005

A finite element model of the electrostatic double layer interaction between an approaching colloidal particle and a small region of a charged planar surface containing four previously deposited particles is presented. The electrostatic interaction force experienced by the approaching particle is obtained by solving the Poisson−Boltzmann equation with appropriate boundary conditions representing this complex geometry. The interaction forces obtained from the detailed three-dimensional finite element simulations suggest that for the many-body scenario addressed here, the electrostatic double layer repulsion experienced by the approaching particle is less than the corresponding sphere−plate interaction due to the presence of the previously deposited particles. The reduction in force is quite significant when the screening length of the electric double layer becomes comparable to the particle radius ($\kappa a \sim 1$). The results also suggest that the commonly used technique of pairwise addition of binary interactions can grossly overestimate the net electrostatic double layer interaction forces in such situations. The simulation methodology presented here can form a basis for investigating the influence of several previously deposited particles on the electrostatic repulsion experienced by a particle during deposition onto a substrate.

1. Introduction

Deposition of colloidal particles on stationary collector surfaces is encountered in a variety of natural and engineered systems, such as colloid transport in subsurface environments, membrane-based water treatment, and chromatography.[1−5] The colloid deposition rate often undergoes temporal variations depending on the nature of the particle−collector and particle−particle interactions.[3,6−14] For a stable suspension of mutually repulsive colloidal particles, the colloid deposition rate generally decreases as the collector surfaces are increasingly covered by deposited particles, a phenomenon generally referred to as blocking.[6,8,11,15] The gradual slowdown of particle deposition rates onto collectors that are partially covered with previously adsorbed particles is a well-studied phenomenon. The colloid deposition dynamics and the extent of surface coverage are strongly influenced by the complex electrostatic double layer interactions between the depositing and the previously deposited particles.[6,10,12−15] Yet, no clearly defined methodology exists to explicitly assess the colloidal interaction forces in a many-body configuration representative of the particle deposition process.

The understanding of colloidal phenomena is primarily based on the Derjaguin−Landau−Verwey−Overbeek (DLVO) interaction potential,[16,17] which is comprised of the Lifshitz−van der Waals (LW) interaction and the electrostatic double layer (EDL) interaction.[18,19] The immense variation of the EDL interaction, brought about by variations in electrolyte concentration of the dispersing medium, pH of the medium, and several other physical and chemical conditions, leads to the diversity of colloidal behavior.[20,21] The primary limitation of the DLVO interaction potential is that it is a pair potential. In other words, this potential represents the interaction between only two colloidal entities suspended in an infinitely large medium. Consequently, it might be unrealistic for many-body geometries encountered in long-term deposition processes, where several previously deposited particles interact simultaneously with a particle approaching a collector.[3,6,8,15,22,23] The theoretical treatments of these systems often neglect the many-body interactions and their role in modifying colloidal phenomena.[21] Even when such

* Corresponding author: tel, (780) 492 6712; fax, (780) 492 2200; e-mail, subir.b@ualberta.ca.

(1) Ryan, J. N.; Elimelech, M. *Colloids Surf., A* **1996**, *107*, 1−56.
(2) Davis, R. H.; Stone, H. A. *Chem. Eng. Sci.* **1993**, *48*, 3993−4005.
(3) Kretzschmar, R.; Borkovec, M.; Grolimund, D.; Elimelech, M. *Adv. Agron.* **1999**, *66*, 121−193.
(4) O'Melia, C. R. *Environ. Sci. Technol.* **1980**, *14*, 1052−1060.
(5) Grolimund, D.; Elimelech, M.; Borkovec, M.; Barmettler, K.; Kretzschmar, R.; Sticher, H. *Environ. Sci. Technol.* **1998**, *32*, 3562−3569.
(6) Johnson, P. R.; Elimelech, M. *Langmuir* **1995**, *11*, 801−812.
(7) Song, L.; Elimelech, M. *Colloids Surf., A* **1993**, *73*, 49−63.
(8) Song, L. F.; Elimelech, M. *J. Chem. Soc., Faraday Trans.* **1993**, *89*, 3443−3452.
(9) Elimelech, M.; O'Melia, C. R. *Environ. Sci. Technol.* **1990**, *24*, 1528−1536.
(10) Liu, D. L.; Johnson, P. R.; Elimelech, M. *Environ. Sci. Technol.* **1995**, *29*, 2963−2973.
(11) Adamczyk, Z.; Siwek, B.; Zembala, M.; Belouschek, P. *Adv. Colloid Interface Sci.* **1994**, *48*, 151−280.
(12) Ryde, N.; Kallay, N.; Matijevic, E. *J. Chem. Soc., Faraday Trans.* **1991**, *87*, 1377−1381.
(13) Ryde, N.; Kihira, H.; Matijevic, E. *J. Colloid Interface Sci.* **1992**, *151*, 421−432.
(14) Privman, V.; Frisch, H. L.; Ryde, N.; Matijevic, E. *J. Chem. Soc., Faraday Trans.* **1991**, *87*, 1371−1375.
(15) Adamczyk, Z.; Warszynski, P. *Adv. Colloid Interface Sci.* **1996**, *63*, 41−149.
(16) Derjaguin, B. V.; Landau, L. *Acta Physicochem. (URSS)* **1941**, *14*, 633−662.
(17) Verwey, E. J.; Overbeek, J. T. G. *Theory of Stability of Lyophobic Colloids*; Elsevier: Amsterdam, 1948.
(18) Russel, W. B.; Saville, D. A.; Schowalter, W. R. *Colloidal Dispersions*; Cambridge University Press: Cambridge, New York, 1989.
(19) Hunter, R. J. *Foundations of Colloid Science*; Oxford University Press: New York, 2001.
(20) Masliyah, J. H. *Electrokinetic Transport Phenomena*; AOSTRA: Edmonton, Canada, 1994; Vol. 12.
(21) Elimelech, M.; Gregory, J.; Jia, X.; Williams, R. *Particle Deposition & Aggregation. Measurement, Modeling and Simulation*; Butterworth-Heinemann, Ltd.: Oxford, England, 1995.

10.1021/la047147e CCC: $30.25
Published on Web 04/07/2005

many-body effects are considered, it is often done in the framework of the pairwise summation principle.[24−27]

Several attempts have been made to investigate the many-body effects on colloidal interactions, especially in a three-body system.[24,27−29] However, a complete and general solution of the electrostatic problem for many-body geometries is still not available. Oberholzer et al.[24] studied the effect of double layer interaction between charged particles near the jamming limit. In their investigation, interaction energies between two particles were calculated for the case of an approaching particle toward another particle previously deposited on a planar surface using a three-body superposition approximation. Their calculations reveal that when the screening length of the electrostatic double layer, κ^{-1}, is much smaller than the particle radius, a (i.e., $\kappa a \gg 1$ or $\kappa a \rightarrow \infty$), the interactions between the particles are not significantly different from what would be obtained from a simple algebraic summation of the pair interactions, even when the particles are very close to the substrate. More rigorous solutions of the many-body Poisson−Boltzmann (PB) problem have been obtained recently.[28,29] It was once again shown that as long as the electric double layer thickness is smaller than the particle radius (i.e., $\kappa a > 1$), there is no significant difference between the forces computed from a rigorous solution of the PB equation for the many-body system and the forces obtained from a superposition of the Yukawa pair potential. All these studies were performed for constant surface charge densities on the particles. On the other hand, when one considers electrostatic interactions between charged colloids in absence of free charges in the intervening dielectric medium, the net force between several interacting particles is computed using the pairwise summation of Coulomb forces. Considering this as the limiting case of electrostatic double layer interactions as $\kappa a \rightarrow 0$, it seems that for both the limits $\kappa a \rightarrow \infty$ and $\kappa a \rightarrow 0$, the electrostatic interactions between many charged particles interacting simultaneously can be expressed as a pairwise summation of the binary interactions.

Recently, we presented results for the electrostatic double layer force between two spheres confined in a cylindrical capillary when the screening length is comparable to the particle radius and for constant surface potentials on the particles.[30,31] In this case, we observed a large deviation in the interaction force between the particles depending on the surface potential of the confining wall (the third body). These results indicate a strong influence of many-body effects on the electrostatic double layer interactions for the case of constant potential particles at low electrolyte concentrations ($\kappa a \sim 1$).

In the present study, a three-dimensional finite element model of electrostatic interactions near a planar wall containing previously deposited particles is presented to obtain the interaction forces experienced by an approaching particle toward a flat collector surface partially covered by four previously deposited particles. The simulations are performed for cases where $\kappa a \sim 1$. A detailed description of the geometry and the mathematical modeling is provided. The problem formulation used in this investigation can be potentially verified using experiments that provide direct force measurement. However, here we have only focused on the numerical prediction of the electrostatic double layer interaction forces for the many-body problem and have compared the detailed simulation results with the commonly used technique of pairwise summation of binary interactions. The finite element simulations presented here provide considerable insight regarding the electrostatic double layer forces between an approaching colloidal particle and a charged planar surface containing previously deposited particles.

2. Mathematical Formulation

In the present investigation, we employ the finite element technique to analyze the interaction force experienced by a charged colloidal particle approaching a charged planar surface (or flat plate) containing previously deposited colloidal particles. The Poisson−Boltzmann (PB) equation is solved with appropriate boundary conditions imposed on the charged particles and the planar surface. In this section, a detailed description of the geometry and a brief description of the mathematical formulation and the boundary conditions of the problem are presented, focusing on some key steps used in the numerical solution.

2.1. Problem Description. A schematic depiction of the computational geometry of a charged particle approaching a planar surface containing four previously deposited particles is shown in Figure 1. Here, four spherical colloidal particles of radius a_{dp} are placed on a charged planar surface separated by a distance (surface-to-surface) of twice the particle radius ($L = 2a_{dp}$). The center-to-center distance between the deposited particles is defined as D. The fifth particle represents the approaching particle (probe particle) of radius a_{pp} located at the origin of the $x-y$ plane. The vertical separation distance between the center of the approaching particle and the planar surface is denoted by z, while the surface-to-surface separation is h ($=z - a_{pp}$), as shown in Figure 1a. The coordinates of the centers of each particle are depicted in Figure 1b. In the finite element modeling, we utilized the symmetry and solved the problem in a computational domain demarcated by the dashed lines in Figure 1b. The resulting computational domain is depicted in Figure 1c.

2.2. Governing Equation and Boundary Conditions. In the framework of the Poisson−Boltzmann equation, the potential distribution around a charged colloidal particle in a symmetric (ν:ν) electrolyte is given by[18]

$$\nabla^2\Psi = \kappa^2 \sinh(\Psi) \qquad (1)$$

Here Ψ ($=\nu e\psi/kT$) is the scaled potential, ν is the valence of the ions, e is the magnitude of electronic charge, ψ is the electrostatic potential, k is the Boltzmann constant, and T is the absolute temperature. The inverse Debye

(22) Bafaluy, J.; Senger, B.; Voegel, J. C.; Schaaf, P. *Phys. Rev. Lett.* **1993**, *70*, 623−626.
(23) Adamczyk, Z.; Siwek, B.; Szyk, L. *J. Colloid Interface Sci.* **1995**, *174*, 130−141.
(24) Oberholzer, M. R.; Stankovich, J. M.; Carnie, S. L.; Chan, D. Y. C.; Lenhoff, A. M. *J. Colloid Interface Sci.* **1997**, *194*, 138−153.
(25) Lowen, H.; Allahyarov, E. *J. Phys.*: *Condens. Matter* **1998**, *10*, 4147−4160.
(26) Ramachandran, V.; Venkatesan, R.; Tryggvason, G.; Fogler, H. S. *J. Colloid Interface Sci.* **2000**, *229*, 311−322.
(27) Russ, C.; von Grunberg, H. H.; Dijkstra, M.; van Roij, R. *Phys. Rev. E* **2002**, *66*.
(28) Dobnikar, J.; Chen, Y.; Rzehak, R.; von Grunberg, H. H. *J. Phys.*: *Condens. Matter* **2003**, *15*, S263−S268.
(29) Dobnikar, J.; Chen, Y.; Rzehak, R.; von Grunberg, H. H. *J. Chem. Phys.* **2003**, *119*, 4971−4985.
(30) Das, P. K.; Bhattacharjee, S.; Moussa, W. *Langmuir* **2003**, *19*, 4162−4172.
(31) Das, P. K. Electrostatic Double Layer Interactions in Confined and Many-Body Geometris. M.Sc. Thesis, Mechanical Engineering, University of Alberta, Edmonton, AB, 2003.

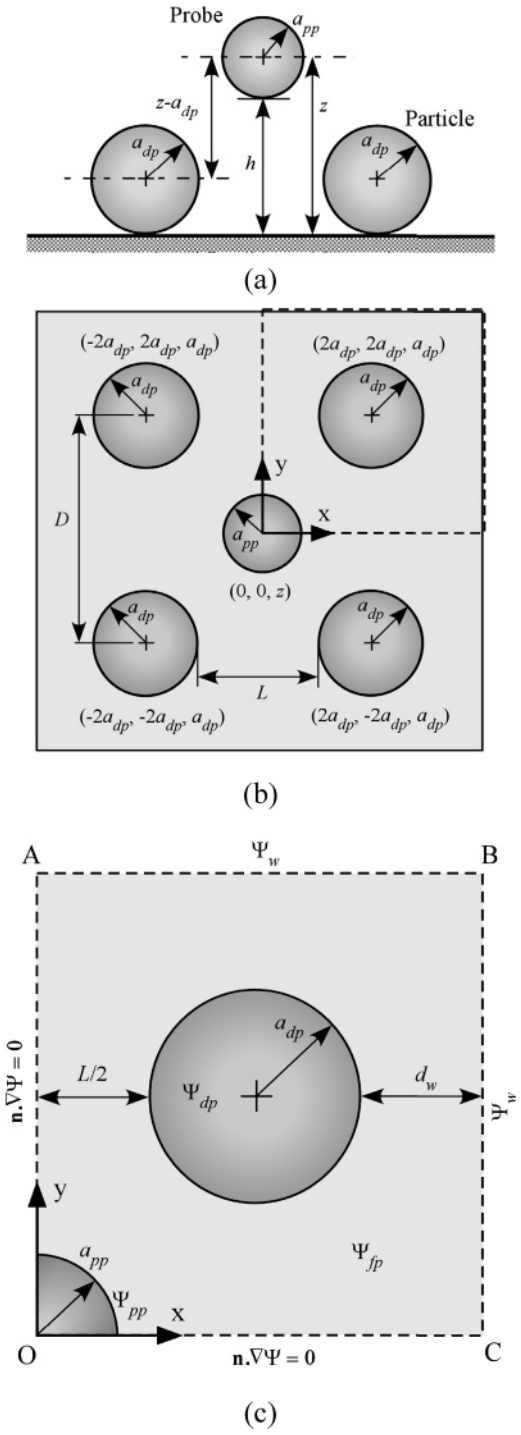

Figure 1. Schematic depiction of a patterned planar surface showing an array of deposited colloidal particles. Part a depicts side view of the geometry under consideration while part b shows a top view along with the coordinates of the center of each particle. The region circumscribed by the broken lines in part b depicts the computational domain under consideration. Part c shows the boundary conditions used in the problem.

screening length, κ, is defined as

$$\kappa = \sqrt{\frac{2n_\infty e^2 \nu^2}{\epsilon\epsilon_0 kT}} \tag{2}$$

where n_∞ is the bulk concentration of the ions (in numbers/m^3), ϵ is the dielectric constant of the suspending fluid, and ϵ_0 is the dielectric permittivity of vacuum.

The surfaces of the charged particles and the planar collector can be assigned constant potential (CP) conditions as

$$\Psi = \Psi_p \tag{3a}$$

for $\partial\Omega \in$ *particle−electrolyte* interface, and

$$\Psi = \Psi_s \tag{3b}$$

for $\partial\Omega \in$ *plate−electrolyte* interface.

One can also employ constant charge (CC) conditions on the surfaces, given by

$$-\mathbf{n}\cdot\nabla\Psi = \sigma_p \tag{4a}$$

for $\partial\Omega \in$ *particle−electrolyte* interface, and

$$-\mathbf{n}\cdot\nabla\Psi = \sigma_s \tag{4b}$$

for $\partial\Omega \in$ *plate−electrolyte* interface.

Here, Ψ_p and Ψ_s represent the scaled surface potentials of the particles and the planar surface, respectively, and σ_p and σ_s are the scaled surface charge densities of the particles and the planar surface, respectively. In our previous studies, it was observed that the electrostatic interaction force between the charged colloidal particles was affected significantly by the proximity of a charged wall for constant surface potential particles.[30,31] Accordingly, in the present investigation, only CP boundary condition on the charged bodies is considered. Here, the surface of the flat plate (bottom wall) is assigned a constant surface potential of Ψ_{fp}, the surfaces of the deposited particles are assigned a constant surface potential of Ψ_{dp}, and the probe particle is assigned a potential of Ψ_{pp}.

On the remaining parts of the boundary (outer domain), we apply the appropriate symmetry boundary conditions as

$$\mathbf{n}\cdot\nabla\Psi = 0 \tag{5}$$

Here, $\mathbf{n}$ represents the unit normal to the surface pointing toward the electrolyte medium. Clearly, eq 5 does not represent the true boundary condition for the top surface and two outer walls of the computational domain. In the numerical solution, an appropriate measure must be taken to ensure that these artificial boundary conditions do not influence the accuracy of the solution by placing these boundaries sufficiently far away from the probe particle and the nearest deposited particle. We also used a somewhat more rigorous boundary condition for the top wall and the two outer walls (AB and BC in Figure 1c) and defined the potential at any point on these walls using linear superposition assumption (LSA) as

$$\Psi_w = \Psi_{fp,1} + \sum_{i=1}^{5} \Psi_{p,i} \tag{6}$$

Here $\Psi_{fp,1}$ represents the potential at any point on the wall due an isolated planar surface defined as[18]

$$\Psi_{fp,1} = 2\ln\left[\frac{1 + \exp(-\kappa h_{fp})\tanh\left(\frac{1}{4}\Psi_{fp}\right)}{1 - \exp(-\kappa h_{fp})\tanh\left(\frac{1}{4}\Psi_{fp}\right)}\right] \tag{7}$$

where Ψ_{fp} is the surface potential of the flat plate and h_{fp} represents the distance between the flat plate and any point on the side wall. $\Psi_{p,i}$ in eq 6 represents the

contribution to the total potential at the wall due to an isolated spherical particle defined as[18]

$$\Psi_{p,i} = \Psi_p \frac{a}{r} \exp[-\kappa(r - a)] \quad (8)$$

where Ψ_p can be either Ψ_{pp} or Ψ_{dp} depending upon the particle location, a is the particle radius (either a_{pp} or a_{dp}), and r denotes the separation distance between the point at which the potential is calculated from the center of particles. Ensuring that the outer walls of the computational domains are sufficiently far away from any of the particles and surfaces allows application of the above linear superposition condition on these boundaries. The LSA boundary condition is used to verify the accuracy of the Neumann boundary conditions used at the outer walls.

2.3. Force Formulation. The three-dimensional nonlinear Poisson−Boltzmann equation was solved in the Cartesian coordinate system to obtain the potential distribution in the electrolyte domain. From the numerically obtained potential distribution, the electrostatic force experienced by the spherical particles can be calculated by integrating the total stress tensor over the particle surface. The stress tensor is comprised of an isotropic osmotic stress contribution and the Maxwell stresses arising from the electrostatic field. Combining these, the electrostatic force on the approaching particle is expressed as

$$\mathbf{F} = \int\int_S \mathbf{T}_{ij}\cdot\mathbf{n}\, dS = \int\int_S \left[\left(\Pi - \frac{1}{2}\epsilon\epsilon_0\mathbf{E}\cdot\mathbf{E}\right)\mathbf{I} + \epsilon\epsilon_0\mathbf{EE}\right]\cdot\mathbf{n}\, dS \quad (9)$$

where the subscript S represents integration over the closed particle surface. Here $\mathbf{F}$ is the force acting on the approaching particle, $\mathbf{T}_{ij}$ is the electrostatic stress tensor, $\mathbf{E}$ ($=-\nabla\psi$) is the electrostatic field vector, Π is the osmotic pressure difference between the electrolyte at the particle surface and the bulk electrolyte, $\mathbf{n}$ is the unit outward surface normal, and $\mathbf{I}$ represents the identity tensor.

The net force acting on the probe particle along the vertical (z) direction can determined from the total force $\mathbf{F}$ and can be written explicitly as

$$F_z = \mathbf{F}\cdot\mathbf{k} = \kappa^2\epsilon\epsilon_0\left(\frac{kT}{ve}\right)^2 \int\int_S \left[E_xE_zn_x + E_yE_zn_y + \frac{1}{2}(-E_x^2 - E_y^2 + E_z^2)n_z\right] dS \quad (10)$$

where $\mathbf{k}$ is a unit vector in the positive z direction, and n_x, n_y, and n_z are the components of the unit surface normal vector $\mathbf{n}$ along the x, y, and z directions, respectively. E_x, E_y, and E_z are the components of the electric field vector $\mathbf{E}$ along the x, y, and z directions, respectively. Utilizing the fact that the integral of the isotropic osmotic pressure term over a closed surface of constant potential vanishes, the net force is evaluated by excluding the osmotic pressure term from eq 9. Finally, the vertical force is calculated in its nondimensional form, given by

$$f_z = \frac{F_z}{\epsilon\epsilon_0}\left(\frac{ve}{kT}\right)^2 \quad (11)$$

The entire simulation procedure was implemented using a finite element software FEMLAB running on a MATLAB (The MathWorks, Inc.) platform in a personal computer (2.4 GHz Pentium IV and 1 GB of RAM).

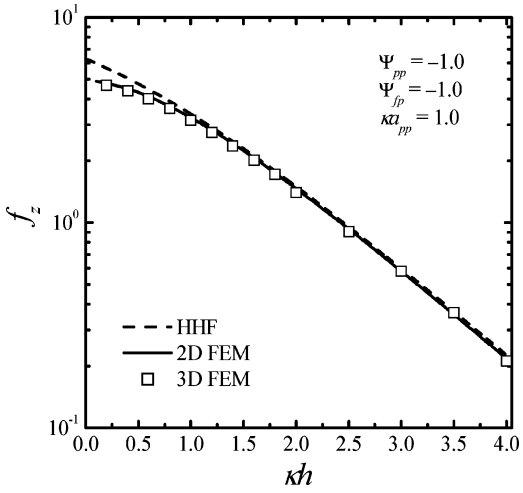

Figure 2. Comparison of the electrostatic double layer interaction force between a charged particle and a charged planar surface obtained from finite element simulation with the corresponding estimates from Hogg et al.[33] The variations of the scaled electrostatic force with scaled separation between the particle and the plate are depicted for a fixed and equal surface potential on both the probe particle and the planar surface ($\Psi_{pp} = \Psi_{fp} = -1.0$). Dashed line represents the result of the analytical HHF (Hogg−Healy−Fuerstenau) expression based on the linearized PB equation, while the solid line represents the result of the two-dimensional finite element method (2D FEM) based on the nonlinear PB equation. Symbols represent the three-dimensional finite element method (3D FEM) results obtained under identical geometry and boundary conditions as the 2D finite element model.

3. Results and Discussion

In this section, we first focus on the accuracy of the three-dimensional (3D) finite element method (FEM) calculations for the limiting case of a charged spherical colloidal particle (the probe) approaching a charged planar surface. Following this, the finite element estimation of the interaction force experienced by an approaching particle toward an array of deposited particles on a flat collector surface is presented. The results from these 3D simulations are then compared against the force estimated using the pairwise summation approach.

3.1. Particle−Plate Interaction. In this subsection, a comparison of the 3D finite element result of the electrostatic force experienced by a charged particle near a charged planar surface is presented with corresponding results available in the literature. This represents a limiting case of the 3D model of the many-body system and provides a validation of the numerical results. In this simple model, a charged colloidal particle (the probe) approaches a bare charged surface (with no deposited particles). This type of geometry can be easily rendered as a two-dimensional (2D) axisymmetric problem in cylindrical coordinates, which can be solved using finite element analysis with a fairly high level of accuracy.[30−32] Furthermore, if one uses the linearized Poisson−Boltzmann equation, the interaction force between the sphere and the planar surface can be obtained analytically for low surface potentials.[33]

The simulation results presented here are obtained for constant potential (CP) conditions on the surfaces of both the particle and the planar surface. Figure 2 depicts a comparison of the interaction forces obtained using the

(32) Das, P. K.; Bhattacharjee, S. *J. Colloid Interface Sci.* **2004**, *273*, 278−290.
(33) Hogg, R.; Healy, T. W.; Fuerstenau, D. W. *Trans. Faraday Soc.* **1966**, *62*, 1638−1651.

detailed 3D simulations, the 2D axisymmetric model, and the analytical expression given by Hogg et al.[33] for constant potential boundary conditions based on the linearized Poisson−Boltzmann equation (this will be referred to as the HHF expression). The nondimensional force between a particle and a flat plate based on the HHF expression can be written as

$$f_{pp-fp} = \pi\kappa a_{pp}(\Psi_{pp}^2 + \Psi_{fp}^2)\left[\left\{\frac{4\Psi_{pp}\Psi_{fp}}{\Psi_{pp}^2 + \Psi_{fp}^2}\right\} \times \frac{\exp(-\kappa h)}{1 - \exp(-2\kappa h)} - \frac{2\exp(-2\kappa h)}{1 - \exp(-2\kappa h)}\right] \quad (12)$$

where $f_{pp-fp} = F_{pp-fp}/\epsilon\epsilon_0(ve/kT)^2$ represents the scaled force, F_{pp-fp} is the net force between the probe particle and the flat plate, Ψ_{pp} and Ψ_{fp} are the scaled surface potentials of the probe particle and the flat plate, respectively, and κh is the scaled surface-to-surface separation distance between the particle and the flat plate. The above expression overestimates the force at small separation distances. However, this expression can predict the interaction force quite accurately at larger separations and low surface potentials.

The particle−plate interaction problem can be solved as an axisymmetric 2D problem using similar techniques as described in our previous work.[30,32] The accuracy of the 2D finite element scheme is already well established based on comparisons with previously calculated results for sphere−sphere interactions.[34,35] In Figure 2, the scaled interaction forces obtained from the 2D finite element calculations based on the nonlinear PB equation (solid line) are compared with the results from eq 12 (dashed line) for a fixed value of the scaled particle size $\kappa a_{pp} = 1.0$ and a fixed and equal dimensionless surface potential $\Psi_{pp} = \Psi_{fp} = -1.0$ on the particle and the plate. The interaction forces obtained from the 2D finite element model agree with the results obtained from the analytical expression over a relatively wide range of scaled separation distances $1.0 < \kappa h < 4.0$. The disagreement between the two solutions at small separation distances is mainly attributable to the overestimation of the force by the HHF expression, which is based on the solution of the linearized PB equation and Derjaguin's approximation. Figure 2 also depicts the scaled interaction forces obtained from the complete 3D simulations (symbols). It is evident that the 3D simulations provide almost identical results as the 2D FEM. Although the above comparison indicates the ability of 3D finite element approximations to provide an accurate estimate of the interaction force, it comes at the expense of fairly involved computation. It should be noted that the results in Figure 2 for the 3D case could only be attained using a large number of elements (usually of the order of 100000) and carefully choosing the convergence and mesh refinement criteria.

3.2. Force Predictions for the Many-Body System: Effect of Boundary Conditions. With the accuracy of the 3D FEM calculations established for the limiting case of a sphere−plate interaction, we now focus on the application of the 3D formulation to the many-body geometry depicted in Figure 1. In this context, it is of interest to first observe how the force estimates can be influenced by application of different artificial boundary conditions (Neumann vs LSA) on the free surfaces of the computational domain. The results shown in Figure 2 were based on an artificial Neumann boundary condition on the outer walls of the computational domain, which is reasonable owing to the symmetry of the sphere−plate geometry. However, as discussed in section 2.2, a Neumann boundary condition might be unrealistic for the many-body geometry. Here we compare the forces obtained using the Neumann condition with those obtained using a more realistic, linear superposition assumption (LSA) based boundary condition on the outer walls of the computational domain.

By application of LSA to define the potentials on the outer walls of the domain (eq 6), the scaled force experienced by the approaching particle at different separation distances was obtained by solving the PB equation employing the 3D finite element model, and the results are plotted in Figure 3a for two different geometrical configurations of the many-body system. The dashed line represents the variation of the scaled interaction force with separation distance for $\kappa a_{pp} = 0.5$, while the solid line shows the forces corresponding to $\kappa a_{pp} = 1.0$. In both cases, the scaled separation distances (d_w, Figure 1c) between the outer wall and the surface of the nearest particle were 2.0 and a scaled surface potential of −1.0 was used on all the charged surfaces. The symbols in Figure 3a, on the other hand, represent the results obtained using the Neumann boundary condition at the top wall and the two outer walls of the computational domain. Two different sets of numerical data (symbols) were obtained using two different separation distances (d_w) between the outer wall and the surface of the nearest particle, as indicated in the legend. From Figure 3a, it is clear that maintaining a sufficient separation ($d_w \geq 2$) between the outer wall and the surface of the nearest particle ensures that both Neumann and LSA based boundary conditions provide virtually identical interaction forces on the probe particle. The percent difference between the forces calculated using Neumann condition and the LSA boundary condition is shown in Figure 3b. The solution of the PB equation for the many-body system with the Neumann boundary condition is generally within 1% of the results obtained using the LSA based boundary condition. Consequently, one might conclude that placing the outer walls at a sufficiently large distance from the nearest particle surface ensures that Neumann boundary conditions on the outer walls can provide sufficiently accurate estimates of the EDL force on the probe particle.

The above comparison provides a critical insight regarding how judicious placement of boundaries in numerical simulations can allow use of simpler boundary conditions (such as Neumann conditions) as approximations to predict the electrostatic interactions with a fair degree of precision. Although approximate, such methods are perhaps the only recourse in multidimensional problem solving schemes in electrostatics, particularly when suitable coordinate transformations that map the infinite domains into a finite computational domain cannot be used. On the basis of the results of Figure 3, we perform all subsequent simulations employing the Neumann boundary conditions at the free surfaces of the computational domain.

3.3. Force Predictions for the Many-Body System: Effect of Previously Deposited Particles. A close inspection of the results shown in Figures 2 and 3a indicates that the interaction force experienced by a probe particle is quite different when it approaches a "clean" planar surface compared to when it approaches a surface containing previously deposited particles. Normally, one would expect that the repulsive force experienced by the probe particle will be less when it approaches a "clean"

(34) Carnie, S. L.; Chan, D. Y. C.; Stankovich, J. *J. Colloid Interface Sci.* **1994**, *165*, 116−128.

(35) Stankovich, J.; Carnie, S. L. *Langmuir* **1996**, *12*, 1453−1461.

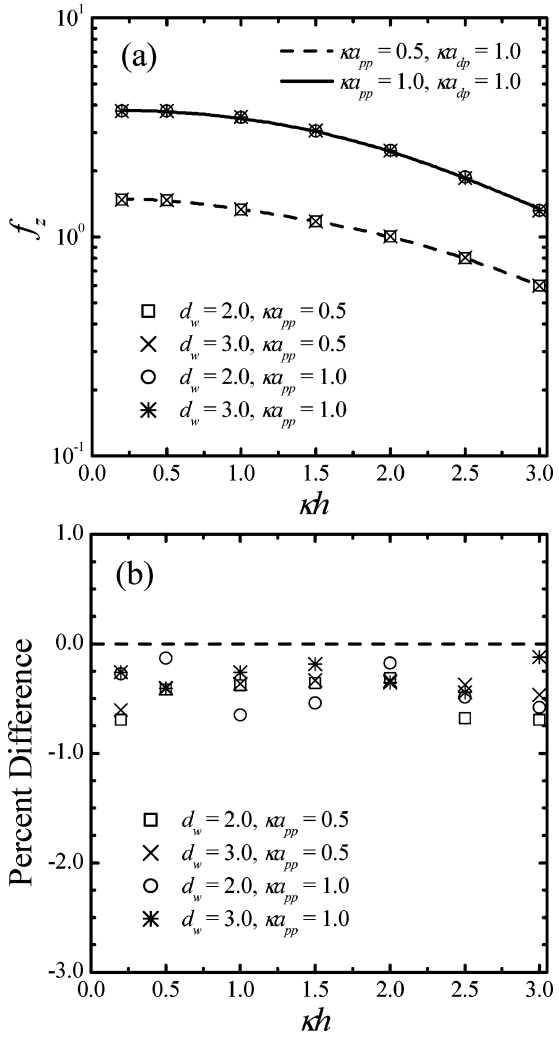

Figure 3. Effect of boundary condition on the finite element estimates of the electrostatic double layer interaction force between a particle and a collector containing previously deposited particles. Two lines in part a represent results obtained using LSA boundary condition on the outer walls of the computational domain for two different sizes of the probe particle as indicated in the legend. Symbols represent the corresponding forces when the outer walls are subjected to the Neumann boundary condition. In both cases, scaled surface potential on the deposited particles, the probe particle, and the flat plate were kept at −1.0. Two different sets of numerical data (symbols) were obtained for each κa_{pp} using two different scaled separation distances (d_w) between the outer wall and the surface of the nearest particle, as indicated in the legend. Part b shows the percent difference between the forces calculated using the Neumann condition and the LSA boundary condition.

charged planar surface compared to the case when it approaches a charged planar surface containing previously deposited charged particles. For a "clean" charged surface, the particle is repelled by the planar surface alone (if both surfaces have similar potentials), while for a surface containing previously deposited particles, the probe particle is repelled by both the planar surface and the deposited particles.

The results of the 3D FEM simulations shown in Figure 4 indicate an opposite behavior at short separation distances. In Figure 4, the interaction force experienced by a probe particle when approaching a clean charged surface is compared against the force on the probe particle when it approaches a charged surface with four previously deposited charged particles. The forces are presented for

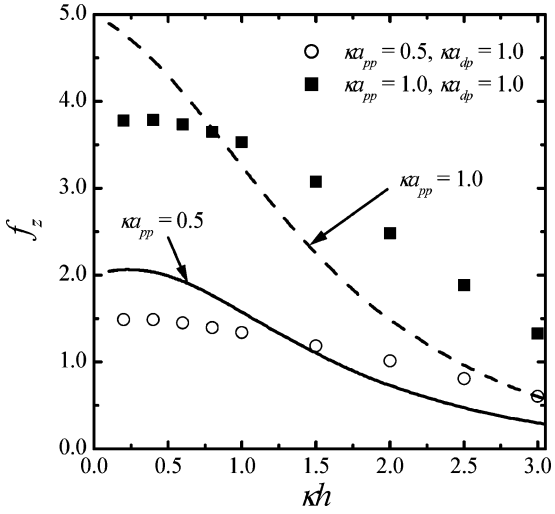

Figure 4. Scaled interaction force experienced by the probe particle when it approaches a "clean" charged planar surface (solid lines) and when it approaches a charged planar surface containing previously deposited charged particles (symbols). The variations of the scaled force with scaled separation distance are depicted for two different sizes of the probe particle as indicated in the legend and a fixed surface potential ($\Psi_{dp} = \Psi_{pp} = \Psi_{fp} = -1.0$) on all the surfaces (particles and collector).

two different sizes of the probe particle as indicated in the legend. Here, the lines represent the variation of the interaction force between a probe particle and a clean planar collector surface with separation distance, while the symbols represent the interaction forces when the probe particle approaches the collector containing previously deposited particles. In all cases, the scaled surface potentials of the particles and the planar surface were −1.0. For both probe particle radii ($\kappa a_{pp} = 0.5$ and 1.0), we observe that at short separation distances, the probe particle feels less repulsion due to the presence of deposited particles compared to the case when no previously deposited particles are present on the planar surface. For instance, comparing the forces experienced by a probe particle ($\kappa a_{pp} = 0.5$) at $\kappa h = 0.6$, we observe that the scaled interaction force is reduced from 1.94 for a clean surface to 1.45 for the partially covered surface, which represents a 25% decrease in the force. Furthermore, the interaction force appears to have become nearly independent of κh for $\kappa h < 0.6$. The significant reduction in the repulsive force as the probe particle comes close to the collector surface is mainly a manifestation of the simultaneous influence of the previously deposited particles. Here the electric field around the probe particle is locally modified and redistributed due to the presence of the previously deposited particles, causing a reduction in the interaction force.

The modifications of electric field around the probe particle can be qualitatively visualized from Figure 5, where maps of the electric field distribution along the diagonal plane (OB in Figure 1c) are shown. Figure 5a depicts the field distribution along the vertical diagonal plane OB for the case when a charged probe particle approaches a bare charged surface (no deposited particles). The other three parts of the figure (b−d) show the electric field ($-\nabla\Psi$) distribution for the case when a charged probe particle approaches the collector surface containing previously deposited particles. Parts a and b of Figure 5 show the field distributions when the scaled separation between the probe particle and the planar surface is $\kappa h = 1.5$, while parts c and d of Figure 5 show the fields for $\kappa h = 1.0$ and $\kappa h = 0.5$, respectively. In all of these figures, the particle

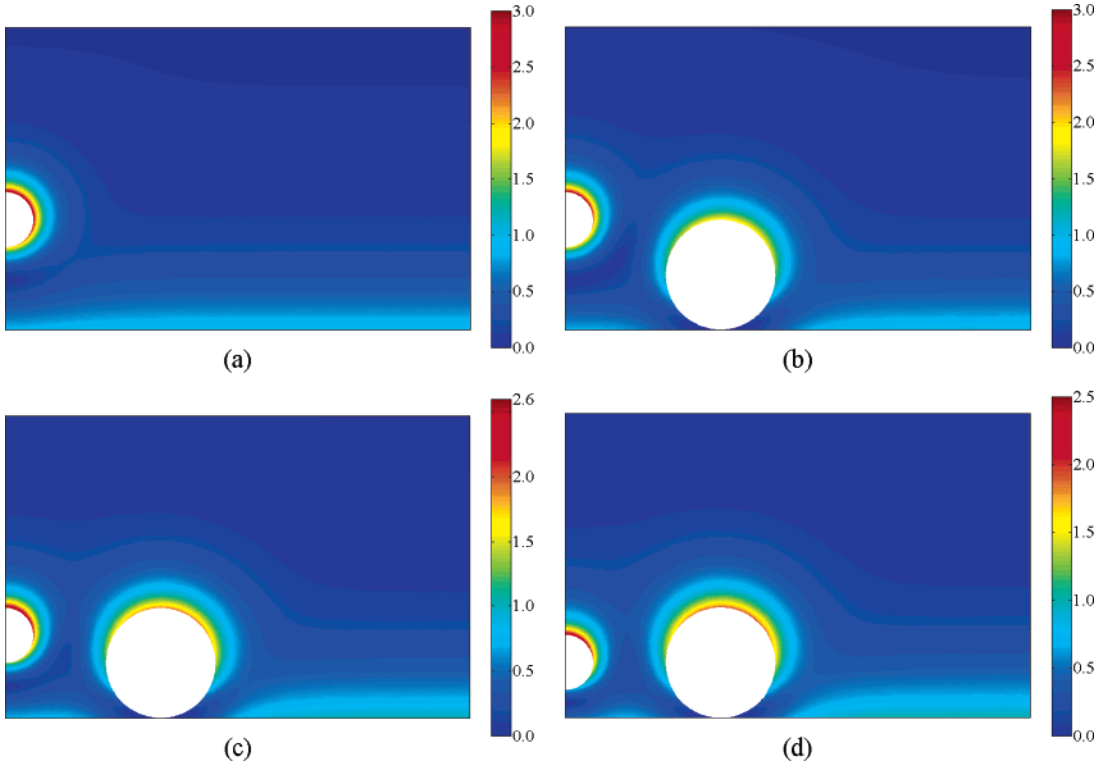

Figure 5. Electric field distribution around the probe particle approaching a "clean" surface in part a and surface with particles previously deposited particles in parts b–d along a vertical diagonal plane OB (Figure 1c). The simulation parameters for all cases are identical except for the presence of the previously deposited particles in parts b–d where $\Psi_{dp} = \Psi_{pp} = \Psi_{fp} = -1.0$. The separation distance between the probe particle and the substrate is $\kappa h = 1.5$ in parts a and b, while the separation distances are 1.0 and 0.5 in parts c and d, respectively.

sizes were $\kappa a_{dp} = 1.0$ and $\kappa a_{pp} = 0.5$, and surface potentials on all the surfaces were fixed at $\Psi_{dp} = \Psi_{pp} = \Psi_{fp} = -1.0$.

It is evident from Figure 5 that the field distribution around the probe particle is considerably modified by the deposited particles compared to the field distribution when the planar surface has no deposited particles. In particular, when one considers the maximum field intensities (shown in red) around the probe particle, it becomes apparent that presence of previously deposited particles reduces the field intensities over the surface of the probe particle facing the planar collector. The reduction in the field intensity is even more pronounced as the probe particle approaches closer to the collector surface (Figure 5c,d). Noting that the electrostatic force on the probe particle is calculated by integrating the Maxwell stress tensor around the probe particle, which is a function of the electric field, it is immediately evident that the net force on the probe particle will diminish owing to the presence of the previously deposited particles. In other words, the presence of the deposited particles will significantly modify the lateral and vertical components of the Maxwell stress, leading to an altered net force experienced by the probe particle.

3.4. Comparison of 3D FEM Simulations with Pairwise Summation Approaches. A simple approach commonly used to estimate the interaction force in many-body geometries is to algebraically sum the pairwise interactions between different entities. In the present case, this approach implies that the total force acting on the probe particle can be represented as the following summation of the pair forces

$$F_{\text{Total,probe}} = F_{\text{pp-fp}} + \sum_{i=1}^{N_{dp}} F_{\text{pp-dp}} \qquad (13)$$

where, $F_{\text{pp-fp}}$ represents the interaction force between the probe and the planar surface, while $F_{\text{pp-dp}}$ represents the force between the probe and the individual spheres deposited on the surface, represented as a simple summation over all the deposited particles (N_{dp}). In the following, we assess the accuracy of two types of pairwise summation approaches by comparing their predictions of the interaction force against the predictions of the 3D FEM based numerical simulations.

In the first pairwise summation approach (referred to as LPB–HHF), an analytical expression is used for the particle–particle and particle–plate interactions based on the solution of the linearized Poisson–Boltzmann (LPB) equation according to Hogg et al.[33] The net interaction force on a probe particle is then obtained by adding the appropriate vertical (along z) components of the individual pair forces. The particle–plate interaction force expression used was given in eq 12, while the particle–particle force for equal surface potential ($\Psi_{pp} = \Psi_{dp} = \Psi$) is given by[33]

$$f_{\text{pp-dp}} = \frac{4\pi\kappa a_{pp} a_{dp} \Psi^2 \exp(-\kappa h)}{(a_{pp} + a_{dp})[1 + \exp(-\kappa h)]} \qquad (14)$$

In the second pairwise summation approach (referred to as NLPB–Hermite), a numerical solution of the nonlinear PB equation based on the Hermite collocation technique is used to calculate the individual particle–particle and particle–plate interactions.[34,35] This NLPB–Hermited pairwise summation approach provides a better estimate of the net force than the LPB–HHF pairwise summation approach, since, for small values of $\kappa a = 1.0$, the nonlinear PB equation provides a more accurate potential distribution. The net force on the probe particle along the vertical (z) direction is obtained by adding

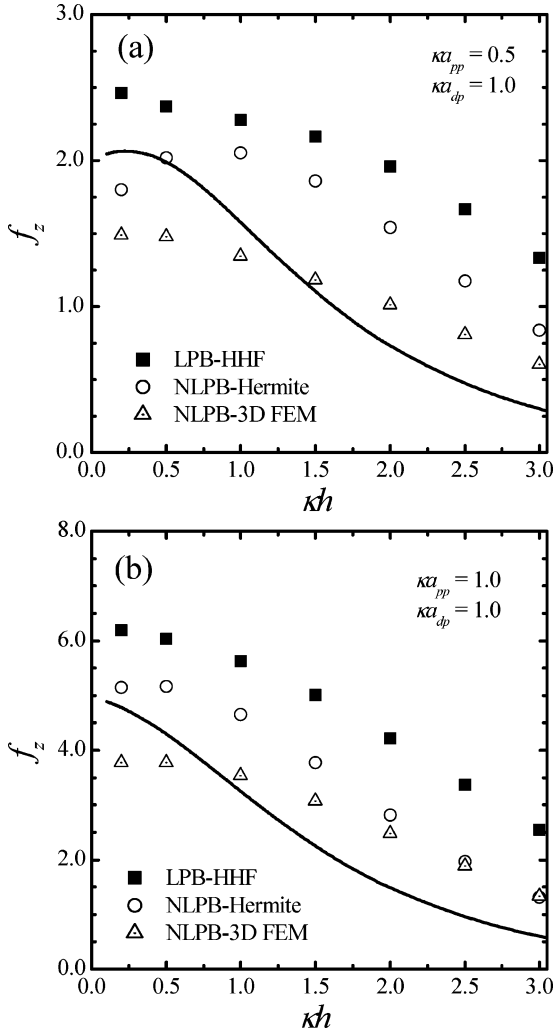

Figure 6. Variation of the scaled interaction force with scaled separation between the probe particle and a particle-covered surface obtained using three approaches (as indicated in the legend) for two different probe particle sizes: (a) $\kappa a_{pp} = 0.5$ and (b) $\kappa a_{pp} = 1.0$. The interaction force experienced by the probe particle when approaching a clean planar surface is shown as a solid line. In both cases, surface potentials of the particles and the planar surface were fixed at −1.0 and the scaled radius of the deposited particles was 1.0.

vertical components of the individual particle−probe and plate−probe forces as

$$f_z = (f_z)_{pp-fp} + 4(f_z)_{pp-dp} \quad (15)$$

A quantitative comparison between the results obtained from the two types of pairwise summation approaches and the corresponding 3D FEM predictions are depicted in Figure 6. The finite element simulation results shown in this figure are obtained for a fixed dimensionless surface potential −1.0 on all the particles and $\Psi_{fp} = -1.0$ on the plate surface for different scaled separation distances. Figure 6a shows the results for $\kappa a_{dp} = 1.0$ and $\kappa a_{pp} = 0.5$, while Figure 6b depicts the case for equal particle sizes ($\kappa a_{pp} = \kappa a_{dp} = 1.0$). It is evident that the 3D FEM simulations in Figure 6 consistently predict lower interaction forces compared to the pairwise summation calculations. The pairwise summation based on LPB gives the highest force, the NLPB based pairwise summation provides a modest (about 15%) reduction in the net force from the corresponding LPB result at $\kappa h = 0.5$, while the 3D FEM results are almost 40% lower than the LPB results and about 30% lower than the forces from the NLPB calculations.

Figure 6 also shows how the forces between the probe and a particle-covered surface computed using the three techniques (symbols) compare against the interaction force between the probe and a clean planar surface (lines). At large separations, all three techniques yield forces that are larger in magnitude than the sphere−plate interaction force. However, as the separation distance becomes smaller, the many-body force predicted by the 3D FEM calculations become smaller than the sphere−plate interaction force (usually for $\kappa h \leq 1.0$). In this context, it is interesting to consider the results at a separation distance of $\kappa h = 0.5$ in Figure 6a. For this separation, since the probe particle size is $\kappa a_{pp} = 0.5$ (half the deposited particle size), the center of the probe particle will be located at the same distance from the substrate as the centers of the deposited particles. If pairwise summation of the interactions holds, it is straightforward to conclude that in this situation the interaction of the probe particle with the substrate will not be affected by the deposited particles. This is evident from the comparison of the NLPB−Hermite pairwise summation result and the sphere−plate interaction for $\kappa h = 0.5$, which are almost identical. However, the 3D FEM result at this separation indicates that the net interaction will be lower than the sphere−plate interaction. This lowering of the interaction force is quite obvious from a consideration of the electric field map shown in Figure 5d, where the presence of the deposited particles modifies the electric field intensities over the upper surface (facing away from the substrate) of the probe particle. Consequently, the Maxwell stresses integrated over the particle surface (and the forces) are considerably modified owing to the presence of the deposited particles even when the probe and deposited particles are aligned at the same vertical distance. It is thus evident that the pairwise summation approaches provide a qualitatively incorrect prediction of the interaction force at close separations between the probe and the particle-covered surface.

So far, we restricted the analysis for low surface potentials, since analytical results based on the linearized PB equation were compared against our numerical results. However, since the 3D FEM solution is obtained for the nonlinear PB equation, it can be applied readily for higher potentials. Figure 7 shows the variation of the scaled interaction force experienced by the probe particle with scaled separation distance, κh, for a fixed particle size ($\kappa a_{pp} = \kappa a_{dp} = 1.0$) using two combinations of the scaled surface potentials on the particles and the planar surface. In this figure, the 3D FEM results (solid lines) are compared with the pairwise summation method based on the Hermite collocation (NLPB−Hermite) technique (dashed lines) for two values of the planar surface potentials ($\Psi_{fp} = -3$ and $\Psi_{fp} = -1$) as indicated in the figure. The symbols represent the corresponding interaction forces between the probe particle and the clean planar surface. For equal surface potentials on the particles and the planar substrate ($\Psi_{dp} = \Psi_{pp} = \Psi_{fp} = -3.0$), the 3D FEM estimates of the forces are always less repulsive compared to the pairwise summation estimates. The second scenario depicted in Figure 7 involves dissimilar surface potentials on the particles and the plate ($\Psi_{dp} = \Psi_{pp} = -3.0$ and $\Psi_{fp} = -1.0$). In this case, the interaction force on the probe becomes attractive at short separations ($\kappa h \leq 0.5$) from the plate. In this scenario, the pairwise summation technique yields a slightly smaller attractive force compared to the 3D FEM results. However, it is interesting to note that in the attractive regions ($\kappa h \leq 0.5$), the predictions based on both the 3D FEM and the

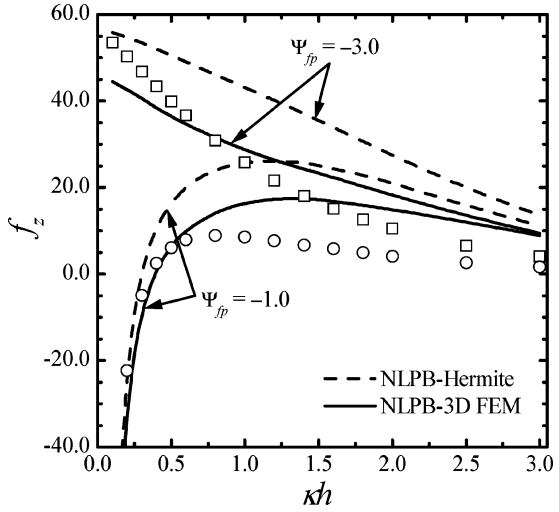

Figure 7. Variation of the interaction force experienced by the probe particle with separation distance for high surface potentials. Solid lines depict interaction force estimated using 3D finite element method, dashed lines represent the results for the NLPB−Hermite method, and symbols show the corresponding particle−plate interactions (squares: $\Psi_{fp} = -3.0$, and circles: $\Psi_{fp} = -1.0$). The simulations were performed for two scaled surface potentials on the planar surface ($\Psi_{fp} = -1.0$ and $\Psi_{fp} = -3.0$) as indicated in the legend, a fixed surface potential on the particle surfaces ($\Psi_{dp} = \Psi_{pp} = -3.0$), and a fixed value of the particle sizes $\kappa a_{dp} = \kappa a_{pp} = 1.0$.

pairwise summation approaches become quite similar to the sphere−plate interaction. These results might have implications on particle deposition behavior in the unfavorable (repulsive interactions) and favorable (attractive interactions) regimes, where the traditional theories based on DLVO approach usually show good agreement with experiments for favorable deposition, while deviating substantially from experimental observations for unfavorable deposition.[21]

The above results indicate the strong influence of the previously deposited particles in modifying the net Maxwell stress around a probe particle as it approaches a particle-covered planar surface. These modified Maxwell stresses significantly lower the net repulsion between the particle and the plate. Consequently, it appears that presence of previously deposited particles can, in fact, facilitate further particle deposition. The phenomenon may also throw some light on the particle deposition behavior on a rough surface. It is known that roughness of a surface enhances particle deposition.[36] Noting that in several of our simulations the deposited particles and the planar surface have the same surface potential, the overall surface containing the deposited particles can be viewed as a model rough surface. In this context, the detailed 3D FEM simulations indeed show that roughness will facilitate deposition by lowering the repulsive electrostatic barrier. One should note that the above observation is valid for cases when the range of the EDL interaction is comparable to the particle radius ($\kappa a \approx 1.0$). Hence, the observations reported here are applicable only for very small particles if one deals with aqueous systems (typically $a_{pp}, a_{dp} < 30$ nm using realistically low electrolyte concentrations). However, in nonaqueous systems, where κ^{-1} is usually much larger, one might encounter such behavior for considerably larger particles.

(36) Hoek, E. M. V.; Bhattacharjee, S.; Elimelech, M. *Langmuir* **2003**, *19*, 4836−4847.

4. Concluding Remarks

A finite element based simulation technique for predicting electrostatic double layer interactions is presented for the approach of a colloidal particle toward a charged planar surface containing previously deposited particles. The simulations performed for the model system reveal that the finite element method would be an excellent tool for such systems. The net EDL force between the approaching particle and a planar collector containing previously deposited particles based on the finite element analysis deviates from the corresponding forces estimated using the pairwise summation principle. From these observations, it seems that the pairwise summation approach commonly used in the literature for assessing the net electrostatic double layer interactions for many-body systems would not be a good approximation for $\kappa a \approx 1$ and at close separations. Our results suggest that in such situations, the pairwise summation method will seriously overestimate the net repulsive electrostatic double layer force experienced by a particle as it approaches a particle-covered surface. The 3D FEM predictions indicate that the repulsive electrostatic double layer interactions in typical unfavorable deposition situations can be substantially modified due to presence of other particles or surface features. For favorable deposition, on the other hand, it is observed that the attractive interactions at short separations are not seriously affected by presence of previously deposited particles. These results might be of some significance in assessing the major discrepancies observed between deposition theories and experimental observations in the presence of repulsive electrostatic double layer interactions.

Glossary

a_{dp}	radius of the deposited particle
a_{pp}	radius of the approaching (probe) particle
d_w	scaled distance between the outer wall and the surface of the nearest particle
D	center-to-center separation distance between deposited particles
e	electronic charge (1.6×10^{-19} C)
$\mathbf{E}$	electrostatic field vector
E_x, E_y, E_z	components of the electric field vector along the x, y, and z directions, respectively
f	scaled force $= F/\epsilon\epsilon_0(ve/kT)^2$
f_{pp-dp}	scaled force between the probe particle and the individual spheres deposited on the planar substrate
f_{pp-fp}	scaled force between the probe particle and the planar substrate
f_z	scaled force acting along the z direction
F_z	component of force acting along the z direction
$\mathbf{F}$	force
h	surface-to-surface separation distance between the probe particle and the planar substrate
$\mathbf{I}$	identity tensor
k	Boltzmann constant (1.38×10^{-23} J K^{-1})
$\mathbf{k}$	unit vector in the positive z direction
L	surface-to-surface separation distance between deposited particles in the $x-y$ plane
$\mathbf{n}$	unit surface normal vector
n_∞	ionic number concentration in the bulk solution (m^{-3})
n_x, n_y, n_z	components of the unit surface normal along the x, y, and z directions, respectively
S	surface of the probe particle

T	absolute temperature (K)
T_{ij}	component of stress tensor

Greek Symbols

∇^2	Laplacian operator
$\partial\Omega$	boundary of the computational domain
ϵ_0	dielectric permittivity in a vacuum (8.8542×10^{-12} C^2 N^{-1} m^{-2})
ϵ	dielectric constant of electrolyte
κ	inverse Debye screening length, eq 2
ν	valency of a symmetric (ν:ν) electrolyte
ψ	electric potential (V)
Ψ	scaled potential ($\nu e\psi/kT$)
Ψ_{dp}	scaled surface potential of the deposited particles
Ψ_{fp}	scaled surface potential of the flat plate
Ψ_p, Ψ_s	scaled surface potential of the particles and the planar surface, respectively
Ψ_{pp}	scaled surface potential of the approaching probe particle
Ψ_w	scaled surface potential of the outer walls based on LSA
Π	osmotic pressure
σ_p, σ_s	scaled surface charge density of the particle and the planar surface, respectively

Abbreviations

CC	constant charge
CP	constant potential
DLVO	Derjaguin−Landau−Verwey−Overbeek
EDL	electrostatic double layer
FEM	finite element method
HHF	Hogg−Healy−Fuerstenau
LSA	linear superposition assumption
LW	Lifshitz−van der Waals
LPB	linearized Poisson−Boltzmann
NLPB	nonlinear Poisson−Boltzmann
PB	Poisson−Boltzmann

Acknowledgment. The authors gratefully acknowledge the financial support from the Canada Research Chairs (CRC) program and the Alberta Ingenuity Fund toward this research. P.K.D. also acknowledges a studentship award from the Alberta Ingenuity Fund and financial support from the Killam Trust.

LA047147E